frontiers | Frontiers in Energy Research

TYPE Original Research
PUBLISHED 01 August 2023
DOI 10.3389/fenrg.2023.1215509

OPEN ACCESS

EDITED BY
Juan P. Amezquita-Sanchez,
Autonomous University of Queretaro, Mexico

REVIEWED BY
Roberto Quintal Palomo,
Universidad Autónoma de Yucatán, Mexico
Carlos Morales Pérez,
Technological University of Puebla, Mexico
Arturo G-P,
University of Guanajuato, Mexico
Agnimitra Biswas,
National Institute of Technology, Silchar, India

*CORRESPONDENCE
Codruta Jaliu,
cjaliu@unitbv.ro
Mircea Neagoe,
mneagoe@unitbv.ro

RECEIVED 02 May 2023
ACCEPTED 10 July 2023
PUBLISHED 01 August 2023

CITATION
Saulescu R, Jaliu C, Neagoe M, Ciobanu D and Cretescu N (2023), Comparative analysis of torque-adding wind energy conversion systems with a counter-rotating vs. conventional electric generator.
Front. Energy Res. 11:1215509.
doi: 10.3389/fenrg.2023.1215509

Comparative analysis of torque-adding wind energy conversion systems with a counter-rotating vs. conventional electric generator

Radu Saulescu[1], Codruta Jaliu[2]*, Mircea Neagoe[2]*, Daniela Ciobanu[2] and Nadia Cretescu[2]

[1]Design of Mechanical Elements and Systems R&D Center, Faculty of Product Design and Environment, Transilvania University of Brasov, Brasov, Romania, [2]Renewable Energy Systems and Recycling R&D Center, Faculty of Product Design and Environment, Transilvania University of Brasov, Brasov, Romania

The paper presents a comparative analysis on the steady-state behavior of two counter-rotating wind turbines with same components, where the generator can operate as a counter-rotating (with both a mobile rotor and stator—*Case a*) vs. conventional (with a fixed stator—*Case b*) electric machine. These wind energy conversion systems (WECSs) also have two coaxial counter-rotating wind rotors and a one-degree-of-freedom (1-DOF) planetary speed increaser with two inputs and one or two outputs for compatibility with the considered generator. The paper aims at highlighting the efficiency and energy performances of WECSs with a counter-rotating vs. conventional generator by investigating three functional scenarios (A, B, and C) of the two WECS cases (*a* and *b*) under the assumption of identical or different counter-rotating wind rotors. A generalized kinetostatic modeling algorithm is first proposed, starting from the general case of WECS with a counter-rotating generator, which allows the establishment of analytical relationships corresponding to speeds and torques at input and output shafts. Numerical simulations of the obtained closed-form model in each scenario highlighted the influence of the constructive parameters on WECS performances, as well as the energetic superiority of WECS, with a counter-rotating generator (*Case a*) vs. conventional generator (*Case b*): higher efficiency by 1.2% and more output power by 1% (Scenario A) to 5.5% (Scenario C).

KEYWORDS

wind turbine, counter-rotating rotors, counter-rotating electric generator, torque-adding speed increaser, modeling, kinematics, statics, operating point

1 Introduction

The European Union (EU) released a revised directive concerning sustainable energy in 2018 (European Union, 2018) which establishes a mandatory objective at the EU level stating that the share of energy from sustainable sources should be at a minimum of 32% until 2030, adding a clause which would allow an ascending revised growth of this percent until 2023 (Windeurope, 2017). Wind energy is the source with the highest percentage of energy production out of the total amount of sustainable energy in EU, and onshore and offshore wind energy is estimated to represent approximately 21% of electric energy production

by 2030. When considering the built environment, a main challenge in designing and implementing wind energy conversion systems (WECS) is to get increased efficiency and energy production that can become main arguments toward choosing sustainable energy.

The growth of energetic performance of wind turbines and optimization of wind potential harnessing can be conducted through different technical solutions converging into one main direction—optimization of the conversion of wind energy into electric energy. This issue refers to the design of either the rotor, gearbox, or electric generator. Thus, the use of multi-rotor systems (Kale and Sapali, 2012) and counter-rotating (primary and secondary) rotors vs. single-rotor (conventional) WECS has proved to harvest more wind energy and, consequently, to increase the electricity production by approximately 40% (Li et al., 2013). Counter-rotating WECS contains two coaxial wind rotors rotating in opposite directions, which can be placed on the same side or on both sides of the nacelle. The primary rotor is the upwind rotor, and the secondary one—the downwind rotor. Vasel-Be-Hagh and Archer (2017) stated that using counter-rotating rotors is 22.6% more efficient in power production than using the single-rotor wind farms, while Circiumaru Oprina et al. (2022) established experimentally the efficiency of counter-rotating WECS on the diameters of the two rotors, with an increase in system efficiency of up to 49.14% being achieved for lower ratios between the diameters of front (upwind) and rear (downwind) rotors. Pacholczyk et al. (2017) demonstrated by simulation that a counter-rotating 5 MW wind turbine brings approximately 20% of additional power compared to the conventional type. Other results refer to the performance of counter-rotating WECS at different aerodynamic loads and blade pitch angles (Jung et al., 2005; No et al., 2009; Rosenberg et al., 2014; Blecharz and Pacholczyk, 2018; Wang et al., 2022), for different number of blades (Pamuji and Bramantya, 2019), various rotor axial distances (Irawan and Bramantya, 2016; Koehuan and SugiyonoKamal, 2017; Pacholczyk et al., 2019), or different rotor configurations (Radhakrishnan et al., 2022). Thus, Rosenberg et al. (2014) demonstrated that the power coefficient for counter-rotating rotors is influenced by the distance between the rotors and their diameters, increasing by 8%–9% when the distance equals the rotor radius and by 7% when the diameter of the upwind rotor is a quarter of the downwind rotor diameter. The pitch control strategy for a 1 MW dual-rotor wind turbine and the impact on its performance were established theoretically (No et al., 2009), both in steady-state and transient regimes, and the results concluded that the proposed model has to be refined by testing the turbine in-site. Li et al. (Zhiqiang et al., 2018) analyzed the improvement of the power coefficient of a micro-counter-rotating wind turbine based on the aerodynamics, the diameters, and configuration of the two rotors and proved that the position of the secondary rotor influences the system efficiency. Moreover, Jung et al. (2005) studied a 30 kW counter-rotating WECS and concluded that the best performance can be obtained when the distance between the rotors is half the auxiliary rotor diameter with the power coefficient reaching 0.5. In addition, it was proved experimentally that the power coefficient decreases with the increase in the pitch angle. A 3 kW coaxial, multi-rotor horizontal-axis wind turbine was built and tested by Mitchell's project team, demonstrating that its power output is approximately three times higher at low and medium wind speeds than a single-rotor turbine of the same diameter (Queen, 2007). All research works concluded that the counter-rotating configuration of rotors is preferable for small power applications rather than the single-rotor WECS.

Regarding the electric generators for WECS, Booker et al. (2010) and Habash et al. (2011) proposed the use of counter-rotating electrical generators for wind turbine applications in urban areas, which have a mobile rotor (*GR*) and mobile stator (*GS*) rotating in opposite directions due to their increased energy performance compared to the conventional (with a fixed stator *GS*) generators. The counter-rotating generator was further investigated in terms of performance and rotor topology by Kutt et al. (2020), Egorov et al. (2021), and Mirnikjoo et al. (2021) and in terms of optimized system configuration with counter-rotating rotors (Mirnikjoo et al., 2020; Ullah et al., 2022a; Ullah et al., 2022b). Cho et al. (2017) analyzedthe performance and control of a WECS with counter-rotating rotors and counter-rotating generator and concluded that this configuration can lower the tip speed ratio at which the power curve attains its maximum almost by half in comparison to the single-rotor system. The designers and developers of counter-rotating generators recommend their use mainly in low-power counter-rotating WECS connected directly to the rotors.

In order to achieve the higher speed requirement of the electric generator, the wind turbines need to include a gearbox for increasing the lower speed of wind rotors. Various types of speed increasers are presented and discussed in the literature: fixed-axis type (Jaliu et al., 2008a; Bevington et al., 2008; Marjanovic et al., 2012), planetary transmissions (Shin, 1999; Jaliu et al., 2008b; Jelaska et al., 2015; Saulescu et al., 2016a; Neagoe et al., 2017; Pastor et al., 2021), and variable speed transmissions (Erturk et al., 2018; Bharani and Sivaprakasam, 2020). Due to their advantages, i.e., high kinematic ratio, reduced radial size, and better efficiency, the researchers consider that the planetary speed increasers are suitable for both single-rotor systems, mainly for the high-power WECS, and for the multi-rotor WECS. For instance, Dong et al. (2017) and Vázquez-Hernández et al. (2017) investigated the parameters that affect the design and the conversion efficiency of WECS and concluded that the use of a planetary transmission is the best option for wind turbines.

In addition, in the counter-rotating WECS configurations, the planetary transmissions can operate either as one-degree-of-freedom (1-DOF) or two-DOF speed increasers, improving in both cases the wind turbine performance. The two operation cases were included by Qiu et al. (2017) in a synthesis of planetary transmissions used in WECS as possible gearboxes, while Saulescu et al. (2018) proposed an algorithm for the conceptual design of the planetary 1-DOF and 2-DOF speed increasers for different functioning situations. Various innovative solutions of planetary speed increasers were proposed (Saulescu et al., 2016b; Saulescu et al., 2018; Neagoe et al., 2019) for counter-rotating WECS. The performance in the steady-state regime of the different WECS configurations was investigated comparatively (Saulescu et al., 2016b; Neagoe et al., 2019; Saulescu et al., 2021; Neagoe and Saulescu, 2022), and a generalized approach for the efficiency analysis of 1-DOF speed increasers for counter-rotating WECS was proposed (Neagoe et al., 2020).

Recent research proved that the use of the counter-rotating generators can lead to a higher conversion efficiency of WECS than the conventional system (Saulescu et al., 2016a; Saulescu et al.,

2016b; Neagoe et al., 2017; Neagoe et al., 2019; Neagoe et al., 2020; Saulescu et al., 2021; Neagoe and Saulescu, 2022). However, only a few studies analyzed WECS configuration with both counter-rotating rotors and counter-rotating generator and proposed suitable mechanical transmissions (Neagoe et al., 2019; Neagoe et al., 2020; Neagoe and Saulescu, 2022). To the best of our knowledge, a major research gap identified in the literature review was the need for comparative analysis of these types of WECS in different structural–functional scenarios that allow their constructive optimization and highlight their benefits in comparison with WECS with a conventional generator.

The paper proposes two WECS configurations that combine the concepts of counter-rotating wind rotors and counter-rotating or conventional electric generator and integrate a novel 1-DOF planetary speed increaser with two inputs and two outputs. The proposed transmission can accommodate both the conventional generator and the counter-rotating generator. The paper proposes a generalized modeling approach of these two types of counter-rotating systems with a counter-rotating generator (*Case a*) vs. conventional generator (*Case b*) and compares their energy performance simulation results in the steady state by considering three scenarios. The same primary rotor and same electric generator are used for both cases in all scenarios, while the secondary rotor is designed as follows:

- Different in the two applications, being established from the condition of achieving the same ratio of input torques k_t (Scenario A).
- Identical to the primary rotor $R1$ but operating at a torque and angular speed (in absolute value) different from $R1$ (Scenario B).
- Identical to the primary rotor $R1$ and operating at a torque and angular speed (in absolute value) identical to $R1$ (Scenario C).

The remainder of the paper is organized as follows: two WECS configurations (*Case a* and *Case b*), consisting of two counter-rotating rotors—a 1-DOF speed increaser and a counter-rotating or conventional electric generator, are proposed in Section 2. Section 3 presents a generalized analytical kinematic modeling, and the torque and efficiency modeling algorithm is proposed in Section 4, based on the input torque ratio k_t. Section 5 deals with the expression of the k_t ratio and the mechanical characteristics of the rotors and generator, while Section 6 provides the expressions of the operating point for the proposed WECS configurations. Section 7 presents the numerical simulations and discussions for the three scenarios, and Section 8 is devoted to final conclusions.

2 Problem formulation

The two WECSs with counter-rotating rotors ($R1$—primary rotor and $R2$—secondary rotor) considered in this comparative study are schematically illustrated in Figure 1. The analysis is based on the following correlation: the second variant (Figure 1B) can be obtained from the counter-rotating system with two outputs (materialized by the rotor *GR* and the stator *GS* of a counter-rotating generator *Gc*, Figure 1A) by breaking the connection between the speed increaser *SI* and the stator *GS* and by fixing the stator (Figure 1B). Therefore, the mathematical models derived in the general case of systems with a counter-rotating generator (*Case a*) allow proving the results obtained for systems with a conventional generator *G* (*Case b*) by customizing the *GS* stator state.

The following assumptions are used in the comparative analysis of the two WECSs:

- Both WECSs use the same mechanical transmission *SI*, for which the following parameters are known: internal kinematic ratio and internal efficiency.
- The same mechanical characteristics are considered for the homologous wind rotors on the one hand and for the electric generators (both conventional and counter-rotating) on the other hand.
- The ratio of the torques of the two wind rotors $k_t = -T_{R2}/T_{R1} > 0$ is introduced; it allows controlling the mechanical characteristic of the rotor $R2$.

The planetary speed increaser (Figure 2) is a complex transmission consisting of two parallel-connected 1-DOF planetary gear sets, 1-2-3-5-6-*H* (PG I = 01) and 4-3-5-6-*H* (PG II = 02), which have three sun gears (1, 4, and 6) and a common planet carrier *H* (Figure 3). The internal kinematic ratios of the two planetary gear sets are denoted by $i_{01} = i_{16}^H = i_{12}^H \cdot i_{23}^H \cdot i_{56}^H = \frac{\omega_1}{\omega_2}\frac{\omega_2}{\omega_3}\frac{\omega_5}{\omega_6} = \left(-\frac{z_2}{z_1}\right)\left(-\frac{z_3}{z_2}\right)\left(+\frac{z_6}{z_5}\right) = +\frac{z_3}{z_1}\frac{z_6}{z_5}$ and $i_{02} = i_{46}^H = i_{43}^H \cdot i_{56}^H = \frac{\omega_4}{\omega_3}\frac{\omega_5}{\omega_6} = \left(+\frac{z_3}{z_4}\right)\left(+\frac{z_6}{z_5}\right) = +\frac{z_3}{z_4}\frac{z_6}{z_5}$, respectively, where z_i is the teeth number of the gear $i = 1\ldots6$ and i_{xy}^z is the kinematic

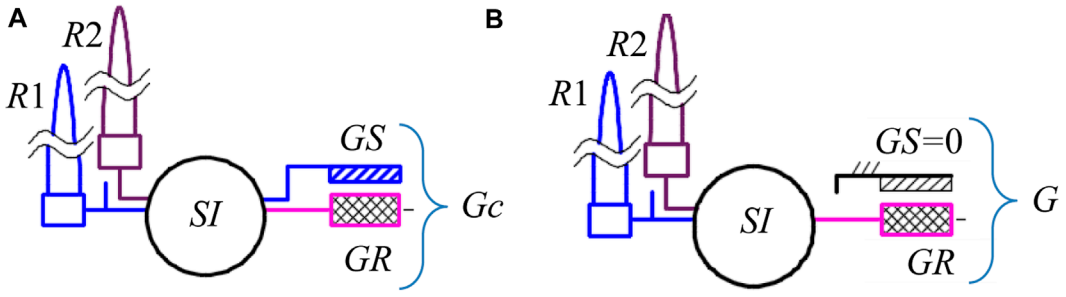

FIGURE 1
Conceptual diagrams of the WECS considered in the comparative analysis: systems with a counter-rotating generator **(A)** and conventional generator **(B)**.

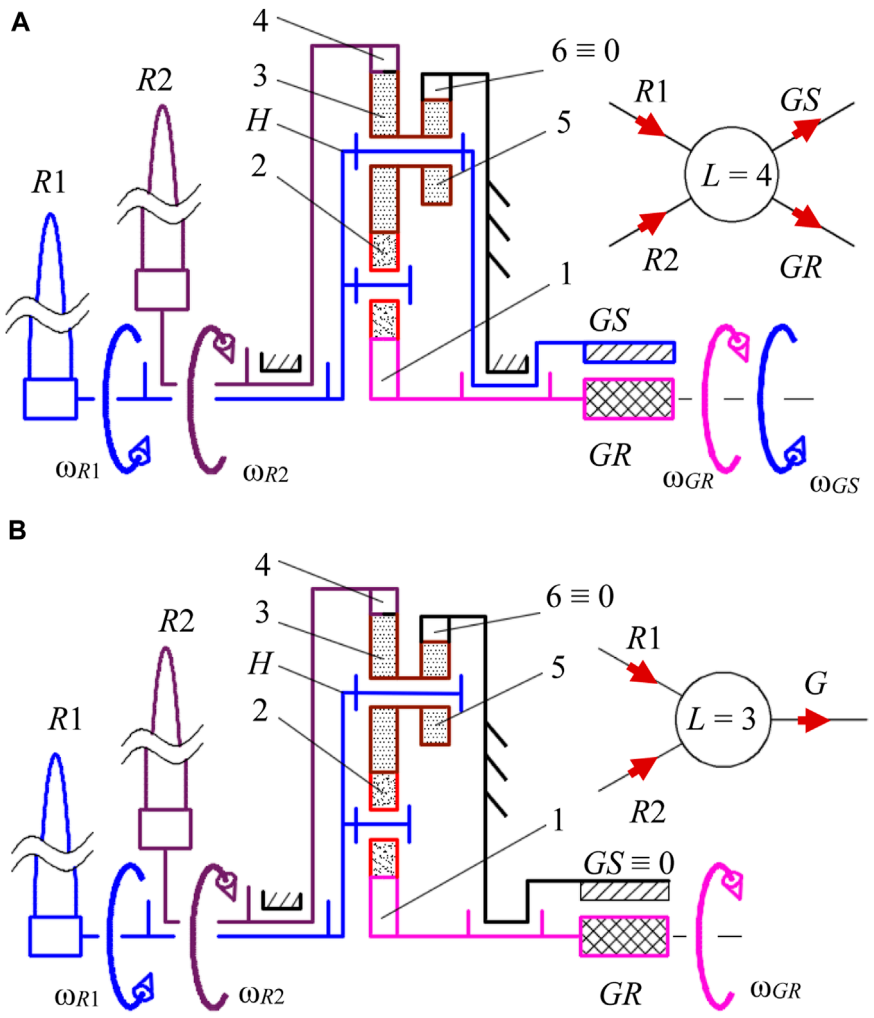

FIGURE 2
Structural schemes and block diagrams of the 1-DOF systems with a counter-rotating generator **(A)** and conventional generator **(B)**.

ratio, where the rotational motion is transmitted from body *x* to body *y* and *z* is considered the reference body.

According to Figure 2A; Figure 3, the WECS with two counter-rotating wind rotors (*R*1 and *R*2), a speed increaser (1-2-3-4-5-6-*H*), and a counter-rotating electric generator *Gc* uses a planetary transmission with two inputs (*H* ≡ *R*1—primary input; 4 ≡ *R*2—secondary input) and two outputs (1 ≡ *GR*—primary output; *H* ≡ *GS*—secondary output). Thus, the 1-DOF planetary speed increaser transmits the mechanical power from the counter-rotating wind rotors to the electric generator whose rotor and stator rotate in opposite directions. This 1-DOF planetary mechanism has the property of a) summing the input torques from the wind rotors (torque-adding) and b) transmission in a determined way of an independent external motion to the other three exterior links. Overall, the planetary transmission (Figure 2A) has four inputs and outputs (*L* = 4): conventionally, the primary input is connected to the wind rotor *R*1, and the secondary input is connected to the wind rotor *R*2; the two outputs are connected to the rotor *GR* and to the stator *GS*. According to Figure 2A, the secondary input *R*2 is connected directly to the stator *GS*. Because the transmission from Figure 2B can be obtained by breaking the connection between the secondary output *H* and the generator stator and by fastening the stator *GS* to the base, its kinematic and static model can be derived as a particular case of the mathematical model of the speed increaser from Figure 2A.

The kinematic and static (torque) correlations, which are systematized in relationships (1)–(3), (4), and (5), refer to the systems shown in Figure 2 and allow highlighting their performance by considering the mechanical characteristics of the wind rotors and the generator or the behavior of one wind rotor in relation to the other. The efficiency of the transmission can be determined either based on the torques of the two wind rotors or by using the torque of the primary rotor (T_{R1}) and the input torque ratio k_t.

3 Kinematic modeling

The specific kinematic correlations of the speed increaser and its connections to the external links can be written according to

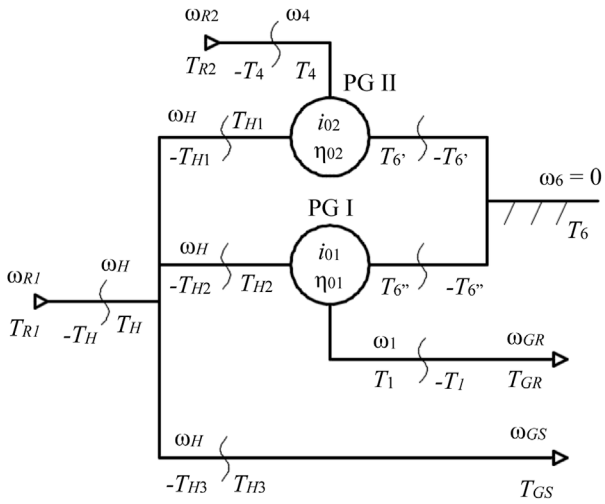

FIGURE 3
Block diagram of the 1-DOF planetary speed increaser with two inputs and two outputs.

Figure 3 starting from the general relationships of a planetary gear set (Neagoe et al., 2020).

Considering the motion of the rotor $R1$ as an independent parameter, Eq. 1 highlights the kinematic correlations specific to the isolated subsystems:

- Input shafts:

$$\omega_{R1} = \omega_H; \quad \omega_{R2} = \omega_4. \tag{1a}$$

- Planetary gear sets:

$$\text{PG I: } \omega_1 - \omega_H(1 - i_{01}) = 0; \quad \text{PG II: } \omega_4 - \omega_H(1 - i_{02}) = 0. \tag{1b}$$

- Transmission connections with the generator stator and rotor:

$$\omega_{GR} = \omega_1; \quad \omega_{GS} = \omega_H. \tag{1c}$$

- The transmission functions of the system:

$$\begin{cases} \omega_{R2} = \omega_{R1}(1 - i_{02}); \\ \omega_{GR} = \omega_{R1}(1 - i_{01}); \\ \omega_{GS} = \omega_{R1}. \end{cases} \tag{1d}$$

Based on the aforementioned equations, the kinematic transmission functions can be obtained as follows:

- 1-DOF speed increaser with two counter-rotating inputs and two counter-rotating outputs, as shown in Figure 2A:

$$\omega_{Gc} = \omega_{GR} - \omega_{GS} = -i_{01}\omega_{R1}. \tag{2}$$

- 1-DOF speed increaser with two counter-rotating inputs and one output, as shown in Figure 2B ($\omega_{GS} = 0$ and $\omega_{GR} = \omega_G$):

$$\omega_G = \omega_{R1}(1 - i_{01}). \tag{3}$$

4 Torques and efficiency modeling

Analogous to the kinematic modeling, the static modeling is performed using the block diagram shown in Figure 3, which allows identifying the static correlations specific to the two planetary gear sets, the equilibrium equations of the links between them and also of the external connections, and the static transmission function. These relationships together with the mechanical characteristics of the wind rotors and the counter-rotating/conventional electric generator can be used for identifying the following: the operating point of the machine of wind rotors—speed increaser—electric generator type; the mechanical power obtained at the input of the electric generator; the power flow through the speed increaser and its efficiency; and the influence of the ratio k_t.

For the 1-DOF speed increaser with two counter-rotating inputs and two counter-rotating outputs, as shown in Figure 2A, the equality $T_{Gc} = T_{GR} = -T_{GS}$ is considered (also valid for the conventional generator) by considering the torque balance for the generator stator and rotor. According to Figure 3, the planetary speed increaser is characterized by the following static correlations starting from its isolated subsystems:

- Input shafts:

$$T_{R1} - T_H = 0; \quad T_{R2} - T_4 = 0. \tag{4a}$$

- Internal shafts:

$$T_H - T_{H_1} - T_{H_2} - T_{H_3} = 0; \quad T_6 - T_{6'} - T_{6''} = 0. \tag{4b}$$

- Planetary gear sets (PG I and PG II):

$$\begin{cases} T_1 + T_{6''} + T_{H_2} = 0; \quad T_4 + T_{6'} + T_{H_1} = 0; \\ T_{6''} = -T_1 \dfrac{i_{01}}{\eta_{01}}; \quad T_{6'} = -T_4 i_{02}\eta_{02}. \end{cases} \tag{4c}$$

- Transmission connections with the generator stator and rotor:

$$T_{GR} - T_1 = 0; \quad T_{GS} + T_{H_3} = 0. \tag{4d}$$

- Transmission functions of the system:

$$T_{GR} = T_{R1}\frac{\eta_{01} - k_t\eta_{01}(1 - i_{02}\eta_{02})}{i_{01}}. \tag{4e}$$

- The mechanical characteristics of the wind rotors and the electric generator:

$$\begin{cases} T_{R1} = -a_{R1}\omega_{R1} + b_{R1}; \\ T_{R2} = -k_t T_{R1} = -a_{R2}\omega_{R2} + b_{R2}; \\ -T_{Gc} = a_G\omega_{Gc} - b_G. \end{cases} \tag{4f}$$

- For the 1-DOF speed increaser with two counter-rotating inputs and one output, as shown in Figure 2B, Eq. 4 is particularized for the fixed stator and $T_{H_3} = 0$:

$$\begin{cases} T_1^* + T_{6''}^* + T_{H_2}^* = 0; \quad T_4^* + T_{6'}^* + T_{H_1}^* = 0 \\ T_{6''}^* = -T_1^* \dfrac{i_{01}}{\eta_{01}}; \quad T_{6'}^* = -T_4^* i_{02}\eta_{02} \\ \\ T_H^* - T_{H_1}^* - T_{H_2}^* = 0; \quad T_6^* - T_{6'}^* - T_{6''}^* = 0; \\ T_{R1} - T_H^* = 0; \quad T_{R2} - T_4^* = 0 \\ T_G - T_1^* = 0 \\ \\ T_G = -T_{R1} \dfrac{\eta_{01} - k_t\eta_{01}(1 - i_{02}\eta_{02})}{\eta_{01} - i_{01}} \\ \\ T_{R1} = -a_{R1}\omega_{R1} + b_{R1}; \quad T_{R2} = -k_t T_{R1} = -a_{R2}\omega_{R2} + b_{R2} \\ -T_G = a_G\omega_G - b_G. \end{cases} \tag{5}$$

In order to avoid possible confusions, the static parameters belonging to the system with a conventional generator, that have different values than those of the first case, are marked with an asterisk.

5 Determination of the k_t ratio

In the general case, the static ratio k_t depends on the input and output mechanical characteristics; a certain value for the k_t ratio can be obtained by modifying appropriately at least one mechanical characteristic. As a result, the analytical expressions of the k_t ratio are further modeled for both systems according to the coefficients of the input and output mechanical characteristics:

- *Case a*, see Figure 2A and Eq. 4:

$$\begin{cases} T_{R2} = -k_t T_{R1}; \\ T_{Gc} = T_{R1} \dfrac{\eta_{01} - k_t\eta_{01}(1 - i_{02}\eta_{02})}{i_{01}}. \end{cases} \tag{6}$$

By replacing the mechanical characteristics presented in Eq. 4 into Eq. 6 and by considering the kinematic correlations from Eqs 1, 2, the following equation system is obtained:

$$\begin{cases} -a_{R2}\omega_{R2} + b_{R2} = a_{R1}k_t\omega_{R1} - b_{R1}k_t; \\ -a_G\omega_{Gc} + b_G = -a_{R1} \dfrac{\eta_{01} - k_t\eta_{01}(1 - i_{02}\eta_{02})}{i_{01}} \omega_{R1} + b_{R1} \dfrac{\eta_{01} - k_t\eta_{01}(1 - i_{02}\eta_{02})}{i_{01}}; \\ \omega_{R2} = \omega_{R1}(1 - i_{02}); \\ \omega_{Gc} = -\omega_{R1} i_{01}. \end{cases} \tag{7}$$

The k_t ratio can be obtained by solving the equation system Eq. 7:

$$k_t = -\frac{a_{R1}b_{R2}\eta_{01} + a_{R2}b_{R1}\eta_{01}(i_{02} - 1) + a_{R2}b_G i_{01}(1 - i_{02}) + a_G b_{R2} i_{01}^2}{a_{R1}[b_{R2}\eta_{01}(i_{02}\eta_{02} - 1) + b_G i_{01}] + b_{R1}[a_{R2}\eta_{01}(i_{02}^2\eta_{02} - i_{02}\eta_{02} - i_{02} + 1) + a_G i_{01}^2]}. \tag{8}$$

By denoting

$$\begin{cases} A = a_{R1}b_{R2}\eta_{01} + a_{R2}b_{R1}\eta_{01}(i_{02} - 1) \\ B = a_{R2}b_G i_{01} \\ C = a_G b_{R2} \\ D = b_{R2}\eta_{01}(i_{02}\eta_{02} - 1) \\ E = a_{R2}\eta_{01}(i_{02}^2\eta_{02} - i_{02}\eta_{02} - i_{02} + 1), \end{cases} \tag{9}$$

it is obtained

$$k_t = -\frac{A + B(1 - i_{02}) + Ci_{01}^2}{a_{R1}[D + b_G i_{01}] + b_{R1}[E + a_G i_{01}^2]}. \tag{10}$$

Case b, see Figure 2B and Eq. 5:

$$\begin{cases} T_{R2} = -k_t T_{R1}; \\ T_G = -T_{R1} \dfrac{\eta_{01} - k_t\eta_{01}(1 - i_{02}\eta_{02})}{\eta_{01} - i_{01}}. \end{cases} \tag{11}$$

Similar to the previous case, by combining Eqs 1, 3, 5 with system (11), it is obtained

$$\begin{cases} -a_{R2}\omega_{R2} + b_{R2} = a_{R1}k_t\omega_{R1} - b_{R1}k_t \\ -a_G\omega_G + b_G = -a_{R1} \dfrac{\eta_{01} - k_t\eta_{01}(1 - i_{02}\eta_{02})}{\eta_{01} - i_{01}} \omega_{R1} + b_{R1} \dfrac{\eta_{01} - k_t\eta_{01}(1 - i_{02}\eta_{02})}{\eta_{01} - i_{01}} \\ \omega_{R2} = \omega_{R1}(1 - i_{02}) \\ \omega_G = \omega_{R1}(1 - i_{01}). \end{cases} \tag{12}$$

The ratio k_t can be determined by solving system (12):

$$k_t = -\frac{A + B(1 - i_{02} - \eta_{01} + \eta_{01}i_{02}) + C(i_{01}^2 + \eta_{01} - i_{01} - i_{01}\eta_{01})}{a_{R1}[D + b_G(i_{01} - \eta_{01})] + b_{R1}[E + a_G(i_{01}^2 - i_{01}\eta_{01} - i_{01} + \eta_{01})]}, \tag{14}$$

where A, B, C, D, and E are defined by Eq. 9.

Taking into account Eqs 2–5, the expressions of the constants a_{R2} and b_{R2} (related to the characteristic of the wind rotor *R2*) are deduced based on the imposed ratio k_t; the following equation can be written from the expression of the k_t ratio:

$$T_{R1}k_t + T_{R2} = 0. \tag{15}$$

An equation of $X\omega_{R1} + Y = 0$ type is obtained from Eq. 15, which leads to

$$[-a_{R1}k_t - a_{R2}(1 - i_{02})]\omega_{R1} + b_{R1}k_t + b_{R2} = 0. \tag{16}$$

As the angular speed ω_{R1} is the independent kinematic parameter, the previous relationship is fulfilled for any value of ω_{R1} only if $X = [-a_{R1}k_t - a_{R2}(1 - i_{02})] = 0$ and $Y = b_{R1}k_t + b_{R2} = 0$; therefore, the coefficients a_{R2} and b_{R2} become

$$\begin{cases} a_{R2} = -\dfrac{a_{R1}k_t}{1 - i_{02}} \\ b_{R2} = -k_t b_{R1}. \end{cases} \tag{17}$$

6 Determination of the operating point

The analytical relationships of the kinematic and static parameters are systematized comparatively in Table 1 for both analyzed WECSs.

The parameters of the operating point (F) reduced on the shaft connected to the generator rotor can be also obtained for the two cases:

- *Case a*, Figure 2A (see Eqs 2, 4):

TABLE 1 Analytical expressions of the kinematic and static parameters.

Parameter		η_{01}	η_{02}	k_t	i_a		η_a	
Relationship					*Case a*	*Case b*	*Case a*	*Case b*
		η_g^3	η_g^2	$-\frac{T_{R2}}{T_{R1}}$	$-i_{01}$	$1-i_{01}$	$\eta_{01}\frac{1-k_t(1-i_{02}\eta_{02})}{1-k_t(1-i_{02})}$	$\frac{\eta_{01}(1-i_{01})}{\eta_{01}-i_{01}}\frac{1-k_t(1-i_{02}\eta_{02})}{1-k_t(1-i_{02})}$
Case a	Parameter	ω_{Gc}			T_{Gc}		P_{Gc}	
	Relationship	$-\omega_{R1}i_{01}$			$T_{R1}\frac{\eta_{01}}{i_{01}}[1-k_t(1-i_{02}\eta_{02})]$		$-\omega_{R1}T_{R1}\eta_{01}[1-k_t(1-i_{02}\eta_{02})]$	
Case b	Parameter	ω_G			T_G		P_G	
	Relationship	$\omega_{R1}(1-i_{01})$			$-T_{R1}\frac{\eta_{01}[1-k_t(1-i_{02}\eta_{02})]}{\eta_{01}-i_{01}}$		$-\omega_{R1}T_{R1}\frac{\eta_{01}(1-i_{01})[1-k_t(1-i_{02}\eta_{02})]}{\eta_{01}-i_{01}}$	

TABLE 2 Values of the parameters related to the steady-state operating point for Scenario (A).

Parameter		ω [s^{-1}]	T [kNm]	P [kW]	ω_{Gc}; ω_G [s^{-1}]	T_{Gc}; T_G [kNm]	P_{Gc}; P_G [kW]	η_a [%]
Case a	*R1*	14.97	113.25	1,696.13	−149.76	10.27	−1,538.71	0.795
	R2	−2.99	−79.27	237.45				
Case b	*R1*	16.57	102.87	1,704.95	−149.16	10.20	−1,522.59	0.783
	R2	−3.31	−72.01	238.69				
a_{R1} = 6.5 kNms; b_{R1} = 210.6 kNm;								
a_{R2} = 22.75 kNms; b_{R2} = −147.42 kNm;								
a_G = 0.11 kNms; b_G = −6.2 kNm.								
i_{01} = 10, i_{02} = 1.2, η_{01} = 0.857, η_{02} = 0.9025, and k_t = 0.7.								

$$\begin{cases} \omega_F = \dfrac{b_G - \frac{b_{R1}\eta_{01}[1-k_t(1-i_{02}\eta_{02})]}{i_{01}}}{a_G + \frac{a_{R1}\eta_{01}[1-k_t(1-i_{02}\eta_{02})]}{i_{01}^2}}; \\ T_F = -a_G\omega_F + b_G; \quad P_F = \omega_F T_F. \end{cases} \tag{18}$$

- *Case b*, Figure 2B (see Eqs 3, 5):

$$\begin{cases} \omega_F^* = \dfrac{b_G + \frac{b_{R1}\eta_{01}[1-k_t(1-i_{02}\eta_{02})]}{\eta_{01}-i_{01}}}{a_G + \frac{a_{R1}\eta_{01}[1-k_t(1-i_{02}\eta_{02})]}{(\eta_{01}-i_{01})(1-i_{01})}}; \\ T_F^* = -a_G\omega_F^* + b_G; \quad P_F^* = \omega_F^* T_F^*. \end{cases} \tag{19}$$

7 Numerical results and discussion

For the purpose of comparative analysis, numerical simulations are further performed by considering that each of the two WECSs is characterized by the internal kinematic ratios $i_{01} = 10$ and $i_{02} = 1.2$ and the internal efficiency $\eta_{01} = \eta_g^3 = 0.95^3 = 0.857$ and $\eta_{02} = \eta_g^2 = 0.95^2 = 0.9025$ for all three scenarios, under following general assumptions:

- The primary rotors *R*1 have the same mechanical characteristic (i.e., same values of a_{R1} and b_{R1}, respectively, see Table 2).
- The electric generators have the same mechanical characteristic in both cases (i.e., same values of a_G and b_G, respectively, see Table 2).

The behavior of the two WECSs is analyzed in three different scenarios, in which the secondary wind rotor and the speed increaser are modified according to the following assumptions:

Scenario (A): the static ratio in both cases is $k_t = 0.7$, achieved by the appropriate selection of the mechanical characteristic of the rotor *R*2.

Scenario (B): the rotors *R*2 of the two WECSs are identical with the rotors *R*1, but different values of k_t are registered for the two cases.

Scenario (C): the rotors *R*2 are identical with the rotors *R*1 in both cases, and the same value of k_t ($k_t = 1$) is obtained for the two WECSs by changing $i_{02} = 2$. In this particular case, the wind rotors *R*1 and *R*2 rotate with equal speeds in opposite directions.

The values of the coefficients $a_{R1,2}$ and $b_{R1,2}$ from the mechanical characteristics of the wind rotors *R*1 and *R*2, which are dependent on the blade aerodynamic behavior, were obtained by applying the algorithm presented in Neagoe and Saulescu (2022). The behavior of the two types of WECSs is further presented comparatively based on the values of the kinematic and static parameters in the operating point, also following the influence of the mechanical characteristics on the system behavior and energy performance.

7.1 Comparative analysis in Scenario A

The coefficients of the mechanical characteristics describing the behavior of the rotors *R*2 are determined based on the previous data, by means of Eq. 17 and imposing $k_t = 0.7$; then, the parameters of the operating points of the two systems are determined based on Eqs 18, 19. The obtained values related to the steady-state operating points are centralized in Table 2 and illustrated in Figures 4–6. The mechanical characteristics of the two wind rotors (Figure 4) are

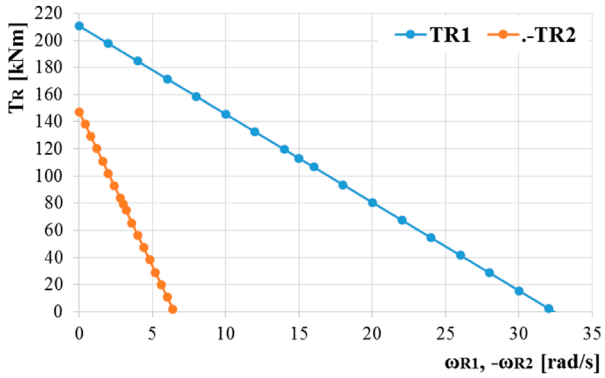

FIGURE 4
Mechanical characteristics of the wind rotors *R1* and *R2* in Scenario A.

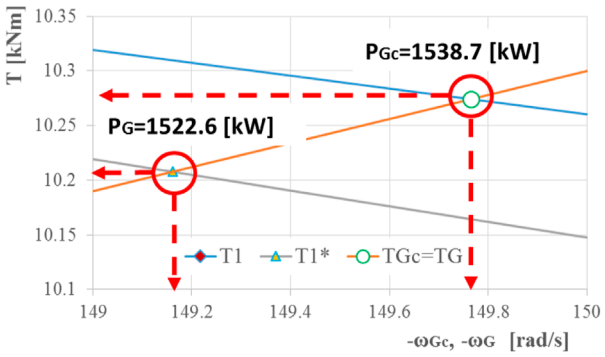

FIGURE 6
Operating points in Scenario A reduced on the generator shafts with the specification of the afferent mechanical power.

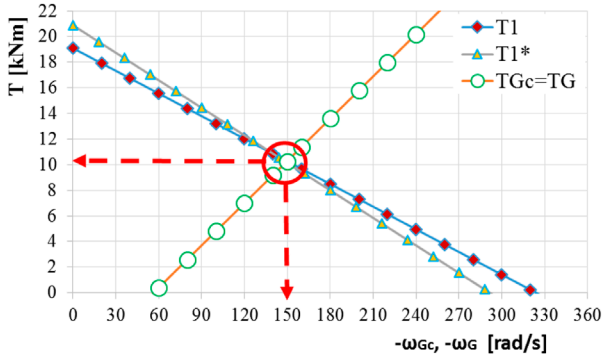

FIGURE 5
Operating points in Scenario A reduced on the shaft of the counter-rotating generator $T_1 = T_{Gc} = T_{Gc}(\omega_{Gc})$ and on the shaft of the conventional generator $T_1^* = T_G = T_G(\omega_G)$.

TABLE 3 Values of the parameters related to the steady-state operating point for Scenario (B).

Parameter	*Case a* (Figure 2A)	*Case b* (Figure 2B)
ω_{R1} [s^{-1}]	15.45	17.14
T_{R1} [kNm]	110.15	99.19
P_{R1} [kW]	1,702.24	1,700.12
ω_{R2} [s^{-1}]	−3.09	−3.43
T_{R2} [kNm]	−190.51	−188.32
P_{R2} [kW]	588.83	645.53
ω_{Gc}; ω_G [s^{-1}]	−154.54	−154.25
T_{Gc}; T_G [kNm]	10.80	10.77
P_{Gc}; P_G [kW]	−1,668.97	−1,661.01
η_a [%]	0.728	0.708
k_t	1.729	1.898
$i_a = \omega_{Gc(G)}/\omega_{R1}$	−10	−9
$a_{R1} = a_{R2} = 6.5$ kNms; $b_{R1} = -b_{R2} = 210.6$ kNm;		
$a_G = 0.11$ kNms; $b_G = -6.2$ kNm.		
$i_{01} = 10$, $i_{02} = 1.2$, $\eta_{01} = 0.857$, and $\eta_{02} = 0.9025$.		

reduced on the *SI* outputs, and thus the operating points in both cases are obtained, as depicted in Figures 5, 6.

Figure 6 details Figure 5 and presents comparatively the two operating points reduced on the transmission output shaft and the afferent mechanical powers. It shows that the output power in *Case a* is higher by ~1% than that in *Case b*, due to the generator benefits of a higher torque and a higher angular speed, implicitly.

From the results systematized in Table 2, it appears that the efficiency of the system with a counter-rotating generator is higher than that of the system with a conventional generator; this aspect is due to the branched transmission of the mechanical power at the output of the speed increaser, in which case the power transmitted to the stator of the electric generator is without friction losses (Figure 3). In the case of the system with a conventional generator, the entire mechanical power is transmitted through the speed increaser only to the rotor of the electric generator, and implicitly, the frictional losses are higher. Therefore, considering a theoretical case of 1 kW cumulative input power generated by the two wind rotors, the 1-DOF transmission with two inputs and two outputs delivers to the generator a power of 795 W, while the system with two inputs and one output delivers a power of 783 W for the same static ratio $k_t = 0.7$.

Due to the higher efficiency in *Case a* compared to *Case b*, an output power $P_{Gc} > P_G$ is obtained despite the lower powers of the rotors *R1* and *R2*, where both rotors operate at lower speeds and higher torques. This phenomenon can be an advantage, especially at lower wind speeds.

7.2 Comparative analysis in Scenario B

The values obtained in this scenario are given in Table 3, by considering identical wind rotors in both cases. Similar to Scenario

TABLE 4 Values of the parameters related to the steady-state operating point for Scenario (C).

Parameter	*Case a* (Figure 2A)	*Case b* (Figure 2B)
ω_{R1} [s^{-1}]	18.42	20.02
T_{R1} [kNm]	90.87	80.45
P_{R1} [kW]	1,673.81	1,610.98
ω_{R2} [s^{-1}]	−18.42	−20.02
T_{R2} [kNm]	−90.87	−80.45
P_{R2} [kW]	1,673.81	1,610.98
ω_{Gc}; ω_G [s^{-1}]	−184.20	−180.18
T_{Gc}; T_G [kNm]	14.06	13.62
P_{Gc}; P_G [kW]	−2,590.33	−2,454.19
η_a [%]	0.773	0.761
k_t	1	1
$i_a = \omega_{Gc(G)}/\omega_{R1}$	−10	−9
$a_{R1} = a_{R2} = 6.5$ kNms; $b_{R1} = -b_{R2} = 210.6$ kNm;		
$a_G = 0.11$ kNms; $b_G = -6.2$ kNm.		
$i_{01} = 10$, $i_{02} = 2$, $\eta_{01} = 0.857$, and $\eta_{02} = 0.9025$.		

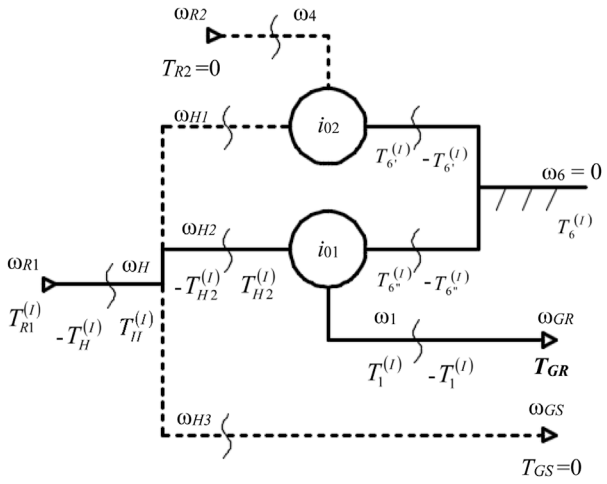

FIGURE 7
Block diagram of the planetary speed increaser from Figure 3 in the functional case of $T_{GR} \neq 0$, $T_{GS} = 0$, and $T_{R2} = 0$.

A, the counter-rotating generator system (*Case a*) achieves a slightly higher power output (by ~0.5%) than *Case b*, as the mechanical power is flowing at a higher efficiency (0.728 vs. 0.708) due to the branched transmission of the output power. Implicitly, the counter-rotating generator operates at higher torque and rotational speed than the conventional generator.

In *Case a*, the rotor *R2* extracts a lower power from wind and the rotor *R1* extracts a higher power than *Case b*. The ratio $k_t > 1$ in both cases (i.e., 1.729 vs. 1.898), that is, the rotor *R2* operates at a higher torque and lower rotational speed than the rotor *R1*.

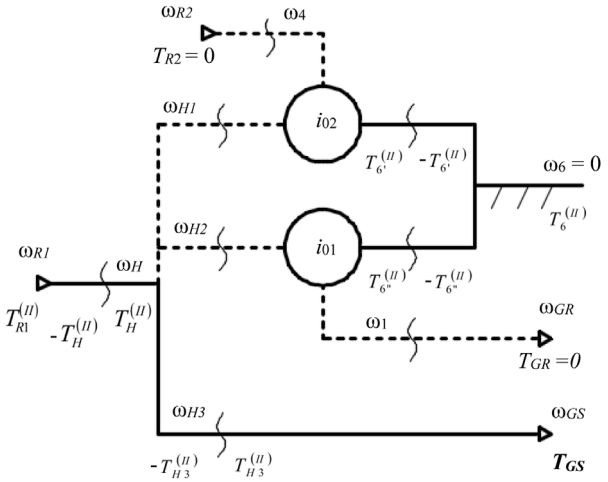

FIGURE 8
Block diagram of the planetary speed increaser from Figure 3 in the functional case of $T_{GR} = 0$, $T_{GS} \neq 0$, and $T_{R2} = 0$.

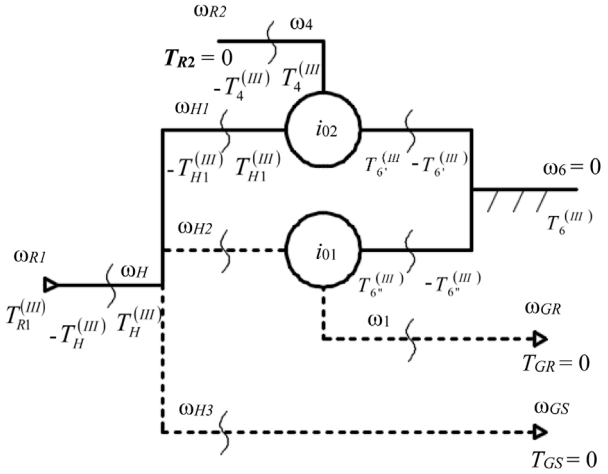

FIGURE 9
Block diagram of the planetary speed increaser from Figure 3, for which the independent torque T_{R2} is considered to be non-zero, i.e., $T_{GR} = 0$, $T_{GS} = 0$, and $T_{R2} \neq 0$.

7.3 Comparative analysis in Scenario C

In order to meet the premise of $k_t = 1$ in both cases, the value of kinematic ratio i_{02} is determined by imposing $\omega_{R2}/\omega_{R1} = -1$ in Eq. 1d:

$$i_{02} = 1 - \frac{\omega_{R2}}{\omega_{R1}} = 2. \tag{20}$$

Table 4 shows the values of the operating points in *Case a* and *Case b* for Scenario C. By imposing the two rotors which rotate in opposite directions with the same speed, an increase in the power supply brought by the rotor *R2* and a better efficiency are obtained compared with Scenario B. The kinematic and static relative behavior of the two cases is similar to the previous

TABLE 5 Expressions of the torques and speeds for the speed increaser with two inputs and two outputs (*Case a*, Figure 3).

	$T_j^{(I)}$ (Figure 7)	$T_j^{(II)}$ (Figure 8)	$T_j^{(III)}$ (Figure 9)	$T_j = T_j^{(I)} + T_j^{(II)} + T_j^{(III)}$
T_{H1}	0	0	$k_t T_{R1}(1 - i_{02}\eta_{02}^{w})$	$k_t T_{R1}(1 - i_{02}\eta_{02}^{w})$
T_{H2}	$-T_{R1}\frac{(1-i_{01}\eta_{01}^{x})[1-k_t(1-i_{02}\eta_{o2}^{w})]}{i_{01}\eta_{01}^{x}}$	0	0	$-T_{R1}\frac{(1-i_{01}\eta_{01}^{x})[1-k_t(1-i_{02}\eta_{o2}^{w})]}{i_{01}\eta_{01}^{x}}$
T_{H3}	0	$T_{R1}\frac{[1-k_t(1-i_{02}\eta_{o2}^{w})]}{i_{01}\eta_{01}^{x}}$	0	$T_{R1}\frac{[1-k_t(1-i_{02}\eta_{o2}^{w})]}{i_{01}\eta_{01}^{x}}$
T_H	$-T_{R1}\frac{(1-i_{01}\eta_{01}^{x})[1-k_t(1-i_{02}\eta_{o2}^{w})]}{i_{01}\eta_{01}^{x}}$	$T_{R1}\frac{[1-k_t(1-i_{02}\eta_{o2}^{w})]}{i_{01}\eta_{01}^{x}}$	$k_t T_{R1}(1 - i_{02}\eta_{02}^{w})$	T_{R1}
ω_H	ω_{R1}			
T_4	0	0	$-k_t T_{R1}$	$-k_t T_{R1}$
ω_4	$\omega_{R1}(1 - i_{02})$			
T_1	$T_{R1}\frac{[1-k_t(1-i_{02}\eta_{o2}^{w})]}{i_{01}\eta_{01}^{x}}$	0	0	$T_{R1}\frac{[1-k_t(1-i_{02}\eta_{o2}^{w})]}{i_{01}\eta_{01}^{x}}$
ω_1	$\omega_{R1}(1 - i_{01})$			
$T_{6'}$	0	0	$k_t T_{R1} i_{02}\eta_{02}^{w}$	$k_t T_{R1} i_{02}\eta_{02}^{w}$
$T_{6''}$	$-T_{R1}[1 - k_t(1 - i_{02}\eta_{o2}^{w})]$	0	0	$-T_{R1}[1 - k_t(1 - i_{02}\eta_{o2}^{w})]$
T_6	$-T_{R1}[1 - k_t(1 - i_{02}\eta_{o2}^{w})]$	0	$k_t T_{R1} i_{02}\eta_{02}^{w}$	$-T_{R1}(1 - k_t)$
ω_6	0			
where $j = H, H1, H2, H3, 1, 4, 6', 6'', 6$, $x = -1$, and $w = +1$.				

scenarios, with the efficiency of the speed increaser with two outputs bringing an improvement of ~1.5%. In this scenario, both rotors *R*1 and *R*2 registered in *Case a* have higher power and torque, accompanied by smaller rotational speed, than those in *Case b*.

7.4 Power flow

Analytically, the static transmission functions can be determined either by solving the system of equations formed by the static relationships from Eq. 4 or using the "effects overlapping" method; according to this method, initially abstracting from the wind rotors and the electric generator, the static analysis of the considered 1-DOF mechanism with $L = 4$ can be reduced (due to its linear-type functions) to the analysis of $L = 3$ simpler 1-DOF mechanisms ($L = 2$); they are obtained from the initially considered mechanism (Figures 2A, 3), leaving non-null in turn for each of the three independent torques: T_{GR}, T_{GS}, and T_{R2}. It is obtained as follows: the mechanism with the block diagram from Figure 7 (with $T_{GR} \neq 0$, $T_{GS} = 0$, and $T_{R2} = 0$), the mechanism from Figure 8 (with $T_{GR} = 0$, $T_{GS} \neq 0$, and $T_{R2} = 0$), and the mechanism from Figure 9, respectively (with $T_{GR} = 0$, $T_{GS} = 0$, and $T_{R2} \neq 0$).

By "overlapping the static effects" of the mechanisms from Figures 7–9, the expressions of the static transmission functions of the initial mechanism (Figure 3) and the torque of the electric generator are obtained. Similarly, the other torques are determined (see Table 5) while being required in the organologic calculations.

As explained in the problem formulation, the 1-DOF speed increaser with two inputs and one output (Figure 2B) was obtained from the speed increaser with two inputs and two outputs (Figure 3) by breaking the stator connection and by fixing it (i.e., $\omega_{GS} = 0$). This speed increaser with one output is a particular case of the one from Figure 3. Its internal torques and speeds are presented in Table 6 by processing the relationships (3) and (5).

TABLE 6 Expressions of the torques and speeds for the speed increaser with two inputs and one output (*Case b*).

T_{H1}^{*}	$k_t T_{R1}(1 - i_{02}\eta_{02}^{w})$
T_{H2}^{*}	$T_{R1}[1 - k_t(1 - i_{02}\eta_{o2}^{w})]$
T_{H3}^{*}	0
T_H^{*}	T_{R1}
ω_H	ω_{R1}
T_4^{*}	$-k_t T_{R1}$
ω_4	$\omega_{R1}(1 - i_{02})$
T_1^{*}	$-T_{R1}\frac{[1-k_t(1-i_{02}\eta_{o2}^{w})]}{1-i_{01}\eta_{01}^{x}}$
ω_1	$\omega_{R1}(1 - i_{01})$
$T_{6'}^{*}$	$k_t T_{R1} i_{02}\eta_{02}^{w}$
$T_{6''}^{*}$	$T_{R1}\frac{[1-k_t(1-i_{02}\eta_{o2}^{w})]i_{01}\eta_{01}^{x}}{1-i_{01}\eta_{01}^{x}}$
T_6^{*}	$T_{R1}\left\{k_t i_{02}\eta_{02}^{w} + \frac{[1-k_t(1-i_{02}\eta_{o2}^{w})]i_{01}\eta_{01}^{x}}{1-i_{01}\eta_{01}^{x}}\right\}$
ω_6	0
where $x = -1$ and $w = +1$.	

A modeling of the power flow from inputs to outputs in both cases is further developed by considering the input power of the primary rotor (P_{R1}) as an independent variable and known values for the input parameters $k_t = 0.7$, $i_{01} = 10$, $i_{02} = 1.2$, and $\eta_g = 0.95$, as used in Scenario A. The correlations corresponding to the speeds and torques for highlighting the power flow in *Case a* (Figure 10) and *Case b* (Figure 11) are obtained by processing Eqs 2, 4, according to Figures 3, 7–9 (see Table 5).

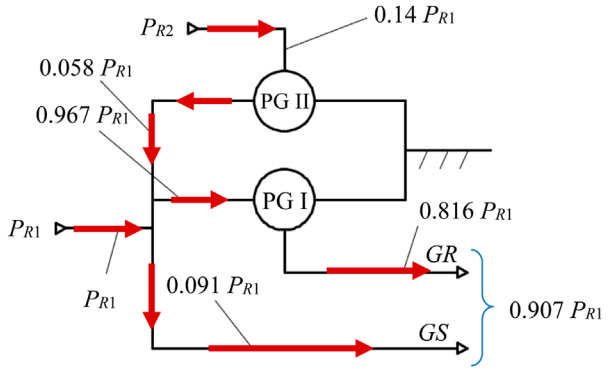

FIGURE 10
Power flow for the 1-DOF speed increaser with two inputs and two outputs (*Case a*).

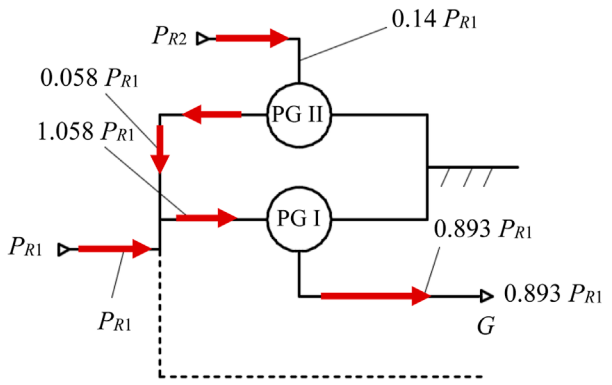

FIGURE 11
Power flow for the 1-DOF speed increaser with two inputs and one output (*Case b*).

In both cases, the rotor *R*2 generates lower mechanical power than the primary rotor (0.14 P_{R1}), which is then directed through the planetary gear set PG II and subsequently connected with power P_{R1}. This cumulative power flows on two branches in *Case a* toward the generator rotor and stator (Figure 10) and is completely directed to the generator rotor in *Case b*, crossing the PG I. Due to the direct transmission of a significant power share to the *GS* (0.091 P_{R1}, Figure 10), the output power in *Case a* is higher than in *Case b* (0.907 P_{R1} vs. 0.893 P_{R1}).

8 Conclusion

The generalized algorithm presented in the paper refers to a 1-DOF planetary transmission with two inputs and two outputs ($L = 4$), used as a torque-adding speed increaser in WECS with two counter-rotating rotors and generator with a mobile stator.

The conclusions drawn from the comparative analysis of the obtained results under the considered premises show the following:

- A WECS with a 1-DOF speed increaser with two counter-rotating outputs achieves a higher efficiency than the WECS with a single output; considering the initial characteristics and a cumulative power of 1 kW at the input, the speed increaser with two counter-rotating outputs brings power gain of 1.2% compared to the case with one output.
- The mechanical characteristics can significantly influence the functionality of a system; for example, the WECS with the set of coefficients defined in Table 2 (Scenario A) achieves a higher efficiency than the homologous WECS with the set of coefficients from Table 3 (Scenario B): by 6.7% more in *Case a* and by 7.7% more in *Case b*.
- The correlation between the speeds of the wind rotors influences decisively their behavior, including static ratio k_t; the increase in the ratio of the wind rotor speeds is accompanied by the increase in the static ratio k_t, as well as input power and output power delivered to the generator, whilst the mechanical efficiency decreases (Table 3 vs. Table 4).

The considered planetary transmission reverses the direction of rotation with respect to the wind rotor *R*1, sums up the input torques, and increases the input speed $i_a = -i_{01}$ times (compared to the motion of the wind rotor R1) while reducing the torque T_{GR}/T_{R1} times.

The efficiency of the 1-DOF transmission with two counter-rotating inputs and two counter-rotating outputs does not depend on the internal kinematic ratio i_{01} (Table 1) and thus on the amplification ratio.

Depending on the power required by the generator and the torque ratio, the proposed algorithm allows determining the mechanical power parameters on each branch, corresponding to the transmission outputs (rotor and stator of the electric generator).

The results of this work are limited to the steady-state behavior of WECS, where constant wind speed is considered and the inertial effects are null, implicitly. The authors intend in the future to address the problem of dynamic modeling and simulation of these WECS types by considering their body moments of inertia and their impact under transitory conditions at variable wind speeds and starting or stopping regimes. It is also intended to experimentally validate the numerical results by developing a specific stand for WECS small-scale prototypes.

Data availability statement

The original contributions presented in the study are included in the article/Supplementary Material; further inquiries can be directed to the corresponding authors.

Author contributions

Conceptualization, RS, CJ, MN, DC, and NC; methodology, RS, CJ, MN, DC, and NC; software, RS, DC, and NC; validation, RS, CJ, MN, DC, and NC; investigation, RS, CJ, MN, DC, and NC; interpretation, RS, CJ, MN, DC, and NC; writing—original draft preparation, RS, CJ, MN, DC, and NC; writing—review and editing,

CJ and MN; supervision, MN and CJ. All authors contributed to the article and approved the submitted version.

Conflict of interest

The authors declare that the research was conducted in the absence of any commercial or financial relationships that could be construed as a potential conflict of interest.

Publisher's note

References

Bevington, C. M., Bywaters, G. L., Coleman, C. C., Costin, D. P., Danforth, W. L., Lynch, J. A., et al. (2008). *Wind turbine having a direct-drive drivetrain*. U.S. Patent 7,431,567 B1.

Bharani, R., and Sivaprakasam, A. (2020). A review analysis on performance and classification of wind turbine gearbox technologies. *IETE J. Res.* 68, 3341–3355. doi:10.1080/03772063.2020.1756936

Blecharz, K., and Pacholczyk, M. (2018). Rotor blade performance analysis for small counter rotating wind turbine. *Zesz. Nauk. Wydz. Elektrotechniki i Autom. Politech. Gdańskiej* 61. doi:10.32016/1.61.13

Booker, J. D., Mellor, P. H., Wrobel, R., and Drury, D. (2010). A compact, high efficiency contra-rotating generator suitable for wind turbines in the urban environment. *Renew. Energy* 35, 2027–2033. doi:10.1016/j.renene.2010.02.003

Cho, W., Lee, K., Choy, I., and Back, J. (2017). Development and experimental verification of counter-rotating dual rotor/dual generator wind turbine: Generating, yawing and furling. *Renew. Energy* 114, 644–654. doi:10.1016/j.renene.2017.06.083

Circiumaru Oprina, G., Chihaia, R., Tanase, N., El-Leathey, A., and Voina, A. (2022). Increasing energy efficiency of counter-rotating wind turbines by experimental modelling. *IOP Conf. Ser. Mater. Sci. Eng.* 1235, 012064. doi:10.1088/1757-899X/1235/1/012064

Dong, H., Zhang, C., Wang, D., Xu, S., and Qiu, J. (2017). Dynamic characteristics of gear box with PGT for wind turbine. *Procedia Comput. Sci.* 109, 801–808. doi:10.1016/j.procs.2017.05.331

Egorov, A., Kaizer, Y., Lysyannikov, A., Kuznetsov, A., Shram, V., Pavlov, A., et al. (2021). Counter-rotating electric generator for wind power plants with liquid metal energy transfer. *J. Phys. Conf. Ser.* 2094, 052018. doi:10.1088/1742-6596/2094/5/052018

Erturk, E., Sivrioglu, S., and Bolat, F. C. (2018). Analysis model of a small scale counter-rotating dual rotor wind turbine with double rotational generator armature. *Int. J. Renew. Energy Res.* 8, 1849–1858. doi:10.20508/ijrer.v8i4.8235.g7549

European Union (2018). Directive (EU) 2018/2001 of the European Parliament and of the Council of 11 December 2018 on the promotion of the use of energy from renewable sources. https://eur-lex.europa.eu/legal-content/EN/TXT/?uri=uriserv:OJ.L_.2018.328.01.0082.01.ENG&toc=OJ:L:2018:328:TOC.

Habash, R. W. Y., Groza, V., Yang, Y., Blouin, Ch., and Guillemette, P. (2011). Performance of a contrarotating small wind energy converter. *Int. Sch. Res. Netw. ISRN Mech. Eng.* 2011, 1–10. doi:10.5402/2011/828739

Irawan, Y., and Bramantya, A. "Numerical simulation of the effect of axial distance between two rotors in counter-rotating wind turbines," in Proceedings of the 2016 2nd International Conference on Science and Technology-Computer (ICST), Yogyakarta, Indonesia, October 2016, 1–5. doi:10.1109/ICSTC.2016.7877338

Jaliu, C., Diaconescu, D. V., Neagoe, M., and Saulescu, R. "Dynamic features of speed increasers from mechatronic wind and hydrosystems. Part II. Dynamic aspects," in Proceedings of the Second European Conference on Mechanism Science EUCOMES 08, Casino, Italy, September 2008.

Jaliu, C., Diaconescu, D. V., Neagoe, M., and Saulescu, R. "Dynamic features of speed increasers from mechatronic wind and hydrosystems. Part I. Structure Kinematics," in Proceedings of the Second European Conference on Mechanism Science EUCOMES 08, Casino, Italy, September 2008.

Jelaska, D., Podrug, S., and Perkušic, M. (2015). A novel hybrid transmission for variable speed wind turbines. *Renew. Energy* 83, 78–84. doi:10.1016/j.renene.2015.04.021

Jung, S. N., No, T.-S., and Ryu, K.-W. (2005). Aerodynamic performance prediction of a 30kW counter-rotating wind turbine system. *Renew. Energy* 30 (5), 631–644. doi:10.1016/j.renene.2004.07.005

Kale, Sandip A., and Sapali, S. N. (2012). Comprehensive evaluation of innovative multi rotor wind turbine designs. *Int. J. Mech. Eng. Technol. (IJMET)* 3 (2), 730–739.

Koehuan, V., and SugiyonoKamal, S. (2017). Investigation of counter-rotating wind turbine performance using computational fluid dynamics simulation. *IOP Conf. Ser. Mater. Sci. Eng.* 267, 012034. doi:10.1088/1757-899X/267/1/012034

Kutt, F., Blecharz, K., and Karkosinski, D. (2020). Axial-Flux permanent-magnet dual-rotor generator for a counter-rotating wind turbine. *Energies* 13, 2833. doi:10.3390/en13112833

Li, Z., Wang, Y., and Xiao, H. "Experimental study on structures of counter-rotating wind turbines," in Proceedings of the ICMREE 2013 - Proceedings: 2013 International Conference on Materials for Renewable Energy and Environment, Chengdu, China, August 2013. doi:10.1109/ICMREE.2013.6893685

Marjanovic, N., Isailovic, B., Marjanovic, V., Milojevic, Z., Blagojevic, M., and Bojic, M. (2012). A practical approach to the optimization ofgear trains with spur gears. *Mech. Mach. Theory* 53, 1–16. doi:10.1016/j.mechmachtheory.2012.02.004

Mirnikjoo, S., Abbaszadeh, K., and Abdollahi, E. (2020). Multi-objective design optimization of a double-sided flux switching permanent magnet generator for counter-rotating wind turbine applications. *IEEE Trans. Industrial Electron.* 68, 6640–6649. doi:10.1109/TIE.2020.3005106

Mirnikjoo, S., Asadi, F., Abbasazdeh, K., and Abdollahi, E. (2021). Effect of rotor topology on the performance of counter-rotating double-sided flux switching permanent magnet generator. *IEEE Trans. Energy Convers.* 37, 65–74. doi:10.1109/TEC.2021.3103555

Neagoe, M., and Saulescu, R. (2022). Comparative energy performance analysis of four wind turbines with counter-rotating rotors in steady-state regime. *Energy Rep.* 8, 1154–1169. doi:10.1016/j.egyr.2022.07.092

Neagoe, M., Saulescu, R., Jaliu, C., and Cretescu, N. (2017). "Novel Speed increaser used in counter-rotating wind turbines," in *New advances in mechanisms, mechanical transmissions and robotics, mechanisms and machine science* (Berlin, Germany: Springer), 143–151.

Neagoe, M., Saulescu, R., and Jaliu, C. (2019). Design and simulation of a 1 DOF planetary speed increaser for counter-rotating wind turbines with counter-rotating electric generators. *Energies* 12, 1754. doi:10.3390/en12091754

Neagoe, M., Saulescu, R., Jaliu, C., and Simionescu, P. A. (2020). A generalized approach to the steady-state efficiency analysis of torque-adding transmissions used in renewable energy systems. *Energies* 13, 4568. doi:10.3390/en13174568

No, T. S., Kim, J.-E., Moon, J. H., and Kim, S. J. (2009). Modeling, control, and simulation of dual rotor wind turbine generator system. *Renew. Energy* 34 (10), 2124–2132. doi:10.1016/j.renene.2009.01.019

Pacholczyk, M., Blecharz, K., and Karkosinski, D. (2017). Modelling of the counter rotating wind turbine. *Proc. XXVII Seminar Organ. by Pol. Soc. Theor. Appl. Electr. Eng. PTETiS, Gdańsk Sect.* 57, 81–84.

Pacholczyk, M., Blecharz, K., and Karkosinski, D. (2019). Numerical investigation on the performance of a small counter-rotating wind turbine. *Energy Mater. Sci. Eng. Energy Syst.* 116, 00055. doi:10.1051/e3sconf/201911600055

Pamuji, D., and Bramantya, A. (2019). Numerical study on the performance of 2-bladed and 3-bladed counter rotating wind turbines. *J. Jpn. Soc. Appl. Electromagn. Mech.* 27, 169–174. doi:10.14243/jsaem.27.169

Pastor, D. G. S. B., Nalianda, D., Sethi, V., Midgley, R., Rolt, A., and Novelo, D. A. B. (2021). Preliminary design framework for the power gearbox in a contra-rotating open rotor. *J. Eng. Gas. Turbines Power* 143, 041022. doi:10.1115/1.4049411

Qiu, J., Liu, B., Dong, H., and Wang, D. (2017). Type synthesis of gearbox in wind turbine. *Procedia Comput. Sci.* 109, 809–816. doi:10.1016/j.procs.2017.05.333

Queen, R. (2007). *Build and test a 3 kilowatt prototype of a coaxial multi-rotor wind turbine*. San Diego, CA, USA: California Energy Commission.

Radhakrishnan, J., Zuber, M., Sridhar, S., Ng, E., and Shenoy, S. "Comparative analysis of counter rotating and conventional vertical axis wind turbine," in Proceedings of the 2022 4th International Conference on Energy, Power and Environment (ICEPE), Shillong, India, April 2022, 1–6. doi:10.1109/ICEPE55035.2022.9798188

Rosenberg, A., Selvaraj, S., and Sharma, A. (2014). A novel dual-rotor turbine for increased wind energy capture. *J. Phys. Conf. Ser.* 524 (1), 012078. doi:10.1088/1742-6596/524/1/012078

Saulescu, R., Neagoe, M., and Jaliu, C. (2018). Conceptual synthesis of speed increasers for wind turbine conversion systems. *Energies* 11, 2257. doi:10.3390/en11092257

Saulescu, R., Neagoe, M., Jaliu, C., and Munteanu, O. (2021). A comparative performance analysis of counter-rotating dual-rotor wind turbines with speed-adding increasers. *Energies* 14, 2594. doi:10.3390/en14092594

Saulescu, R., Neagoe, M., Jaliu, C., and Munteanu, O. (2016b). Comparative analysis of two wind turbines with planetary speed increaser in steady-state. *Appl. Mech. Mater.* 823, 355–360. doi:10.4028/www.scientific.net/AMM.823.355

Saulescu, R., Neagoe, M., Munteanu, O., and Cretescu, N. (2016a). Performance analysis of a novel planetary speed increaser used in single-rotor wind turbines with counter-rotating electric generator. *Mater. Sci. Eng. – IOP Conf. Ser. Mater. Sci. Eng.* 147 (1), 012090. doi:10.1088/1757-899X/147/1/012090

Shin, C. (1999). *Multi-unit rotor blade system integrated wind turbine*. U.S. Patent 5,876,181.

Ullah, W., Khan, F., and Hussain, S. (2022a). A comparative study of dual stator with novel dual rotor permanent magnet flux switching generator for counter rotating wind turbine applications. *IEEE Access* 10, 8243–8261. doi:10.1109/ACCESS.2022.3143166

Ullah, W., Khan, F., and Hussain, S. (2022b). Dual mechanical port power distribution in dual rotor permanent magnet flux switching generator for counter-rotating wind turbine applications. *IET Renew. Power Gener.* 16, 1267–1277. doi:10.1049/rpg2.12450

Vasel-Be-Hagh, A., and Archer, C. (2017). Wind farms with counter-rotating wind turbines. *Sustain. Energy Technol. Assessments* 24, 19–30. doi:10.1016/j.seta.2016.10.004

Vázquez-Hernández, C., Serrano-González, J., and Centeno, G. (2017). A market-based analysis on the main characteristics of gearboxes used in onshore wind turbines. *Energies* 10, 1686. doi:10.3390/en10111686

Wang, K., Liu, T., Wan, Y., Ong, M. C., and Wu, T. (2022). Numerical investigation on aerodynamic characteristics of dual-rotor wind turbines. *J. Mar. Sci. Eng.* 10, 1887. doi:10.3390/jmse10121887

Windeurope, (2017). Wind energy in europe: Scenarios for 2030. https://windeurope.org/wp-content/uploads/files/about-wind/reports/Wind-energy-in-Europe-Scenarios-for-2030.pdf.

Zhiqiang, L., Yunke, W., Jie, H., Zhihong, Z., and Wenqi, C. (2018). The study on performance and aerodynamics of micro counter-rotating HAWT. *Energy* 161, 939–954. doi:10.1016/j.energy.2018.07.049

Nomenclature

a_G	speed coefficient in the generator mechanical characteristic
a_R	speed coefficient in the wind rotor mechanical characteristic
b_G	torque term in the generator mechanical characteristic
b_R	torque term in the wind rotor mechanical characteristic
DOF	degree of freedom
F	operating point
G	conventional electric generator
Gc	counter-rotating electric generator
GR	generator rotor
GS	generator stator
H	satellite carrier
i_0	internal kinematic ratio
i_a	speed amplification ratio
i^z_{xy}	kinematic ratio where the rotational motion is transmitted from body x to body y and z is considered as the reference body
k_t	ratio of the input torques
L	total number of inputs and outputs
P	power
P*	power for the system with a conventional electric generator
PG	planetary gear set
R1*/*R2	primary/secondary wind rotor
T	torque
T*	torque for the system with a conventional electric generator
η	efficiency
η_0	internal efficiency
η_a	WECS overall efficiency
η_g	efficiency of a gear pair
ω	angular speed
ω^*	angular speed in the case of the system with a conventional electric generator
SI	speed increaser
WECS	wind energy conversion system
z_i	number of teeth of gear i